1 Extending the vadose zone: Characterizing the role of snow for liquid

2 water storage and transmission in streamflow generation

3

- 4 Ryan W. Webb ^{1,2,3}, Keith N. Musselman ³, Siobhan Ciafone ⁴, Katherine E. Hale ^{3,4}, and
- 5 Noah P. Molotch ^{3,4}
- 6 Department of Civil, Construction, and Environmental Engineering, University of New
- 7 Mexico, Albuquerque, New Mexico, USA
- 8 ² Center for Water and the Environment, University of New Mexico, Albuquerque, New
- 9 Mexico, USA
- ³ Institute of Arctic and Alpine Research, University of Colorado Boulder, Boulder,
- 11 Colorado, USA
- ⁴ Geography Department, University of Colorado Boulder, Boulder, Colorado, USA

13

- 14 Corresponding Author: Ryan Webb, Center for Water and the Environment, University of
- 15 New Mexico, Albuquerque, New Mexico, USA
- 16 Email: rwebb@unm.edu

17

18 Abstract

- 19 Streamflow response in headwater catchments is highly sensitive to the hydrologic
- 20 connectivity of hillslopes to streams during spring snowmelt. Despite strong evidence at
- 21 point- to plot-scales of flow paths creating lateral connectivity within an alpine snowpack,
- 22 meltwater is commonly assumed to infiltrate vertically through the snowpack. Hydrologic
- 23 models only treat the horizontal (downstream) routing of water once released from the
- snowpack and/or soil column. This assumption limits our ability to represent the full dynamic
- 25 nature of hydrologic connections in snow-dominated mountainous headwaters. Thus, the goal
- of this study is to assess the mechanisms that control the spatiotemporal distribution of liquid
- 27 water in an alpine snowpack during the spring snowmelt season. We utilize terrestrial laser
- scanning (TLS), ground penetrating radar (GPR), and manual observations to map the
- 29 seasonal dynamics of snow depth, snow water equivalent (SWE), and within-snow liquid
- water content (LWC). We compare these observations to point-scale parameter sensitivity
- analyses with a modular snow model (SUMMA). The results show high spatial variability of
- 32 LWC in an alpine snowpack during snowmelt. Statistical analyses show LWC is most highly
- correlated to snow depth ($r^2 = 0.62$). However, including the distance to bare soil and

topographical slope slightly improved the coefficient of determination (r² = 0.67). While hydrologic models have the flexibility to simulate many of the observed dynamics in snowpack liquid water storage, model simulations using previously published parameter ranges always underestimated the high liquid water storage at one of the three sites. This is likely a result of current model structures that lack capabilities for surface ponding of water within a snowpack or surface runoff laterally through a snowpack. Our slope-scale characterization of the spatiotemporal distribution of in-snow LWC, together with a model-based sensitivity assessment, will inform future efforts in hydrologic model development and catchment observations. **Keywords:** Snowmelt Retention, SUMMA, Hydrologic Flow paths

1. INTRODUCTION

48

49

50

51

52

53

54

55

56

57

58

59

60

61

62

63

64

65

66

67

68

69

70

71

72

73

74

75

76

77

78

79

80

81

Seasonal snow accumulation and melt are critical components of the hydrologic cycle in mountainous areas with important controls on climate, ecosystem function, flood risk, and water resources (Bales et al., 2006). Globally, over one billion people rely on water that originates as snow (Barnett, Adam, & Lettenmaier, 2005) with continuing increases in both demand for and value of that water (Wada & Bierkens, 2014). In mountainous headwater basins, more than 85% of annual precipitation can accumulate as a winter snowpack. In the western United States, seasonal snowmelt produces two-thirds of total inflow to reservoirs (Li, Wrzesien, Durand, Adam, & Lettenmaier, 2017). Historical trends and 21st century projections indicate that as air temperatures continue to warm, snowpack will decline and winter snowmelt will become more frequent (Knowles, Dettinger, & Cayan, 2006; Musselman, Addor, Vano, & Molotch, 2021; Stewart, Cayan, & Dettinger, 2004). This earlier snowmelt is projected to occur at slower rates due to the shift towards a time of lower available energy (Musselman, Clark, Liu, Ikeda, & Rasmussen, 2017). Assessments of the potential socioeconomic and environmental impacts of ongoing and projected changes in snowmelt timing and magnitude require consideration of physical processes by which snowmelt water becomes available for streamflow.

Changes in the timing and rate of meltwater (i.e., the snowmelt pulse) have profound implications on seasonal soil moisture (Harpold et al., 2015; Webb, Fassnacht, & Gooseff, 2015), evapotranspiration (ET) (Winchell, Barnard, Monson, Burns, & Molotch, 2016), groundwater recharge (Ford, Kendall, & Hyndman, 2020), downstream water availability (Vano et al., 2014), and rain-on-snow flood risk (Musselman et al., 2018). Streamflow and groundwater recharge respond nonlinearly to input of snowmelt such that slight reductions in snowmelt rates may disproportionately reduce runoff (Barnhart et al., 2016; Musselman, Molotch, & Margulis, 2017). However, our understanding of these potential impacts remains conceptual in nature through the use of hydrologic models. However, these hydrologic models need further verification of physical processes in complex terrain during snowmelt to ensure appropriate representation of the important processes. Improved process-level understanding of physical hydrologic processes during snowmelt is needed to properly structure ecohydrologic models. In this context, improvements to model structure are needed to simulate the interactions amongst snow distribution, melt, ET, runoff, and more broadly, to assess the sensitivity of snow-dominated regions to climate change. One key source of uncertainty is our relatively limited knowledge of the dynamic pathways of snowmelt in headwater systems – how meltwater moves from melting snow grains to the soil system.

The hydrologic connectivity of hillslopes to streams greatly impacts streamflow response (e.g. Detty & McGuire, 2010; Jencso et al., 2009; McGlynn & McDonnell, 2003; McNamara, Chandler, Seyfried, & Achet, 2005). We conceptualize two types of hydrologic connectivity: static and dynamic. Static connectivity is related to the landscape architecture that can be categorized and mapped (e.g., the 'plumbing' of hydrologic response units). Dynamic connectivity refers to variations in antecedent wetness and storage capacity that facilitates and buffers streamflow, ultimately producing a nonlinear response to inputs (Bracken & Croke, 2007). Hillslopes have both static and dynamic connectivity that operate simultaneously to generate streamflow. In snow-dominated catchments, these concepts of static and dynamic hydrologic connectivity have been limited to near-surface groundwater dynamics (e.g. Gasemizade & Schirmer, 2013; Jencso & McGlynn, 2011; McNamara et al., 2005). To date, there has been little focus on the hydrologic connectivity that occurs because of liquid water storage and transport within and among the layers of a seasonal snowpack in mountainous terrain. Despite strong evidence of lateral connectivity of liquid water within snow (e.g. Eiriksson et al., 2013; Webb, Wigmore, Jennings, Fend, & Molotch, 2020; Williams, Rikkers, & Pfeffer, 2000), meltwater is commonly assumed to infiltrate vertically and only mobilize horizontally once at or below the snow-soil interface (Fig. 1; e.g. Clark, Nijssen, & Luce, 2017; Kormos et al., 2014). This assumption may limit our ability to represent the full dynamic nature of hydrologic connections in snow-dominated mountainous headwater systems (Brauchli, Trujillo, Huwald, & Lehning, 2017) needed to simulate snow water resources and the ecohydrologic sensitivity to climate change.

103104

82

83

84

85

86

87

88

89

90

91

92

93

94

95

96

97

98

99

100

101

102

[Insert Figure 1]

105106

107

108

109

110

111

112

113

114

115

To represent snowmelt infiltration more accurately across a landscape, it is beneficial to consider snow as a layered porous media with unsaturated flow dynamics occurring during spring snowmelt (Webb, Jennings, Finsterle, & Fassnacht, 2021). Snow is a complex, three-dimensional matrix of ice, air, liquid water, and constituents (e.g., dust). The hydraulic properties of snow layers depend on crystal structure, snow density, and relative saturation (i.e., liquid water content). These dynamic properties are determined by the meteorological conditions under which snow layers are deposited and subsequently evolve (Colbeck, 1991; Domine, Morin, Brun, Lafaysse, & Carmagnola, 2013; Hirashima, Avanzi, & Wever, 2019; Wever, Fierz, Mitterer, Hirashima, & Lehning, 2014; Yamaguchi, Watanabe, Katsushima, Sato, & Kumakura, 2012) that vary across a catchment by elevation, wind exposure, slope,

aspect, and vegetation (Elder, Dozier, & Michaelsen, 1991; López-Moreno, Fassnacht, Beguería, & Latron, 2011; Molotch, Colee, Bales, & Dozier, 2005; Sexstone & Fassnacht, 2014). Similar to soils, the hydraulic properties of snow layers can form hydraulic barriers (Webb, Fassnacht, Gooseff, & Webb, 2018), translating meltwater tens of meters downslope (Eiriksson et al., 2013; Liu, Williams, & Caine, 2004; Peitzsch, Birkeland, & Hansen, 2008), and creating complex hydrologic flow paths (Kampf, Markus, Heath, & Moore, 2015; Webb, Jennings, Finsterle, & Fassnacht, 2021; Webb, Williams, & Erickson, 2018; Williams, Erickson, & Petrzelka, 2010). Unlike flow paths through soils, which can be conceptualized as a mix of static and dynamic components, all flow paths through snow are dynamic because the physical snowpack structure evolves at sub-daily timescales. To date, the ever-changing nature of flow paths through snow has limited our understanding to what can be directly observed at small scales (i.e., cm to m) (e.g. Williams et al., 2010; Leroux, Marsh, & Pomeroy, 2020) with only recent advances using remote sensing techniques applied at plotscales (up to tens of meters) (e.g. Webb et al., 2020). As remote sensing tools continue to evolve, it is critical to advance our understanding of how liquid water in snow evolves at the hillslope and catchment scales.

The goal of this study is to assess the mechanisms that control the spatiotemporal distribution of liquid water in an alpine snowpack during the spring snowmelt season. We answer the following research questions: 1) What factors control the storage of liquid water in snow? 2) How does the liquid water storage in snow change throughout the snowmelt season? And 3) How accurately do hydrologic models simulate the observed snowpack liquid water storage?

To address these questions, we use terrestrial laser scanning (TLS), ground penetrating radar (GPR), and manual observations to map the seasonal dynamics of snow depth, snow water equivalent (SWE), and the within-snow liquid water content (LWC) in an experimental alpine headwater catchment. Leveraging these unique observations, we conduct point-scale parameter sensitivity analyses with a modular snow model to compare the observation-based estimates of snow LWC to the simulated ranges. Our slope-scale characterization of the spatiotemporal distribution of liquid water in a melting alpine snowpack, together with a model-based sensitivity assessment, will inform future efforts in hydrologic model development and catchment observations.

2. METHODS

2.1 Study Site

This study was conducted in an alpine headwater catchment at the Niwot Ridge Long Term Ecological Research (LTER) study site near Boulder, Colorado. The Saddle catchment (SDL) is instrumented with a meteorological station that records hourly measurements of shortwave and longwave radiation, wind speed, barometric pressure, air temperature, and relative humidity (Jennings, Kittel, Molotch, & Yang, 2021). An ultrasonic sensor near the station records measurements of snow depth every 30-minutes (Morse et al., 2021). Hourly precipitation and SWE is measured ~2 km away at the University Camp SNOTEL site.

Decades of work in SDL include water flow through snow (Webb et al., 2020; Williams et al., 2010; Williams et al., 2000), hydrograph separation (Hill, 2017; Liu et al., 2004), groundwater modelling (Evans, Ge, Voss, & Molotch, 2018), biogeochemical processes (Knowles et al., 2015; Williams, Seibold, & Chowanski, 2009), and ecological processes (e.g. Wieder, Knowles, Blanken, Swenson, & Suding, 2017). Nearby laboratory facilities are maintained on the ridge of SDL providing storage, line power, and access to this otherwise remote catchment.

The SDL research catchment is approximately 0.3 km² with elevations ranging from 3400 to 3650 m asl and 80% of the area above treeline (Fig. 2a). The terrain has generally modest slopes and a predominantly southeast aspect, creating an environment largely affected by strong westerly winds. Wind deposition of snow occurs on leeward slopes (SE and E aspects) and wind scour on windward slopes (SW and W aspects). Streamflow discharge in SDL has been monitored for over two decades (Williams et al., 2015) with recent hydrochemistry analysis indicating more than 60% of annual runoff derives from snowmelt that lacks geochemical evidence of interaction with the local geology (Hill, 2017).

For this study, the SDL catchment was monitored for the spatial and temporal distribution of liquid water storage within the snowpack during the 2019 melt season. During this melt season, peak SWE in the SDL catchment occurred on approximately 17-May. The observation period of this study occurred between 14-May and 27-June with a total of 3 terrestrial lidar scans and 11 GPR surveys. The timing of these surveys targeted early and peak snowmelt.

[Insert Figure 2]

2.2 Snow Depth Estimates

The spatial distribution of snow depth (d_s) was determined using established TLS methodology (e.g. Deems, Painter, & Finnegan, 2013). TLS data were collected on 14-May,

7-June, and 27-June with a Riegl VZ-6000 lidar scanner from three scan positions to capture the area of interest. Georeferencing and aligning multiple scans was accomplished using Trimble Business Center and Riegl RiSCAN Pro software packages. Ground surface (i.e., snow-free) scans occurred on August 20, 2019. Scans were georeferenced using four 16.5 cm diameter reflective targets with Trimble R10 rover GPS units corrected to a Trimble NetR9 base station with a Zephyr Geodetic antenna. Post-processing estimates of TLS absolute accuracy are \sim 0.02 m. The TLS surfaces were aggregated to produce 3 m resolution digital elevation models (DEMs) of the ground and snow surfaces. For each scan date, d_s was calculated by subtracting the ground surface DEM from the snow surface DEMs.

To estimate the spatial snow depth patterns on dates when TLS observations were not available, temporal interpolation was applied to leverage information from TLS and continuous d_s observations from the ultrasonic sensor. For accumulation events, the relative distribution of event-based snow accumulation was assumed to follow the same spatial pattern as that observed near peak accumulation from the 14-May TLS data collection. Thus, the maximum accumulation d_s field, as observed by TLS, was normalized relative to the observed d_s at the SDL ultrasonic sensor on 14-May (Fig. 3). Similarly, ablation was assumed to occur in the spatial pattern observed as the difference of d_s fields from the 14-May and 7-June TLS scans. These assumptions regarding the spatial patterns of spring accumulation and melt were assessed by comparing ultrasonic d_s values measured at the SDL site against the University Camp SNOTEL site located ~2 km away (Fig. 3c). In the comparison between the two sites, consistent relationships in spring snow accumulation and melt would result in a linear trend when the daily d_s values are plotted against each other. A linear regression fit to the data has an r^2 value of 0.89 indicating this method to be acceptable, particularly since all points of interest at the SDL site are much closer to the depth sensor than the SNOTEL site.

[Insert Figure 3]

2.3 Ground Penetrating Radar

We used GPR data collection to obtain further information of snowpack properties (e.g., Marshall, Koh, & Forster, 2005). A GPR pulse is an electromagnetic wave that travels through the snowpack and is reflected off changes in material properties such as density, with the strongest reflection often from the snow-soil interface (Bradford, Harper, & Brown, 2009; Holbrook, Miller, & Provart, 2016; Webb, 2017). For this study, two-way-traveltime (t_2) of GPR waves through snow were obtained along transects on eight survey dates: 17-May, 23-

May, 27-May, 31-May, 7-June, 14-June, 20-June, and 27-June. We used a Mala Geoscience, Inc. ProEx control unit pulse GPR system with an 800 MHz shielded antenna. The antenna was fixed in place on a plastic sled towed behind a user or between two users. A GPS antenna connected to the ProEx control unit registered location information every second. Transect end points were marked with 2.5 cm diameter, 2 m long plastic pipes inserted halfway into the snow to maintain a repeatable travel path each survey.

Radar pulses were triggered on 0.05 s intervals using eight times stacking. The average survey travel speed was \sim 0.5 m/s resulting in \sim 40 returns per meter. The ReflexW 2D Software package was used for time-zero adjustment, taken as the first break in the first wavelet, a dewow filter, and spherical divergence correction to compensate for signal attenuation. The dewow filter removes low frequency content by calculating a running mean that is subtracted from a central point. The reflection of the snow-soil interface was then picked at the first break prior to the first peak of the reflection. Topography was corrected for by dividing t_2 by the cosine of the ground surface slope at that location. Distributed t_2 data were aggregated to a 3 m raster using the mean of t_2 values, to match the distributed d_s maps.

2.4 Estimating Liquid Water Content

The effective dielectric permittivity (ε_{eff}) of snow is sensitive to snowpack density and LWC (Bradford et al., 2009; Heilig et al., 2015; Webb, Jennings, Fend, & Molotch, 2018), and is calculated from the observed velocity (ν) of the radar wave through snow:

$$\varepsilon_{eff} = (S/v)^2$$
 Eq (1)

where s is the speed of light in a vacuum (~ 0.3 m/ns) and v is calculated using:

$$v = \frac{d_s}{\left(\frac{t_2}{2}\right)}$$
 Eq (2)

241 where d_s is the distributed snow depth estimates derived from TLS as described in section 242 2.2.

The bulk volumetric LWC (θ_w) of snow is calculated from ε_{eff} (Eq. 1) using the Roth et al. (1990) three phase mixing model that is commonly applied (Heilig et al., 2015; Koch, Prasch, Schmid, Schweizer, & Mauser, 2014; Mitterer, Heilig, Schweizer, & Eisen, 2011; Schmid et al., 2015; Webb, Jennings, et al., 2018):

$$\theta_{w} = \frac{\varepsilon_{eff}^{0.5} - \frac{\rho_{d}}{\rho_{i}} \varepsilon_{i}^{0.5} - \left(1 - \frac{\rho_{d}}{\rho_{i}}\right) \varepsilon_{a}^{0.5}}{\varepsilon_{w}^{0.5} - \varepsilon_{a}^{0.5}}$$
Eq (3)

where ρ_d is the density of dry snow, ρ_i is the density of ice (917 kg m⁻³), ε_i , ε_a , and ε_w are the dielectric permittivities of ice, air, and liquid water, respectively. At 0°C these dielectric

permittivities are known ($\varepsilon_i = 3.18$, $\varepsilon_a = 1.0$, and $\varepsilon_w = 87.9$). For this study, we observed ρ_d through manual snow pit measurements at two locations within SDL, one near the depth sensor on a flat aspect and one near a deep snow drift on a southern aspect slope. Snow pit observations in this study were only used to obtain bulk density estimates using a 1000 cm³ wedge cutter and digital scale with 1 g precision. The density observations were made in 10 cm vertical increments to provide a density profile that was averaged for the bulk density. The methods described above result in an estimated accuracy for θ_w of ~0.02. When applying equation 3 to the SDL catchment, we set a maximum θ_w value of 0.30 due to the lack of studies confirming permittivity equations for snow with such high values of liquid water storage. For more information concerning this method, see Webb et al. (2018).

2.5 Snowpack Modelling

The snowpack was modelled with the Structure for Unifying Multiple Modelling Alternatives (SUMMA) (Clark, Fan, et al., 2015; Clark, Nijssen, Lundquist, Kavetski, Rupp, Woods, Freer, Gutmann, Wood, Brekke, et al., 2015; Clark, Nijssen, Lundquist, Kavetski, Rupp, Woods, Freer, Gutmann, Wood, Gochis, et al., 2015). SUMMA is a hydrologic model that provides flexibility to experiment with different hydrologic model decisions including spatial representations, flux parameterizations, and parameter values. One-dimensional (i.e., point) simulations were conducted at three locations selected to represent the basin range of slope, snow depth, and snow cover persistence in the SDL catchment. Table 1 summarizes the site characteristics. In SUMMA, in-snow LWC and transmission are estimated as a function of snow temperature, volumetric ice content, and gravity drainage, with consideration of capillary retention processes within the pore space of a snow layer.

Elevation, slope, and aspect were derived from a 10 m airborne lidar-derived DEM (Anderson, Guo, & Parrish, 2013). Local soils and geological surveys conducted in SDL (Hill, 2017) were used to define the model discretization and initial conditions of eight soil layers to a total depth of 4 m. The lower soil boundary conditions were specified as a zero-flux for the soil thermodynamics and free-draining for the soil hydrology. Vegetation was classified as tundra and was buried by snow-cover. Except for precipitation, which is described below, hourly meteorological variables from the SDL station were used to force the model. Due to a sensor error, measured incoming longwave radiation was unavailable and was estimated using a parameterization based on SDL station measurements of air temperature, relative humidity, and incoming shortwave radiation (Schmucki, Marty, Fierz,

& Lehning, 2014). Measured shortwave radiation was projected onto the slope of each point simulation.

Wind speed at each site was estimated from measurements at the SDL station using a linearized, spatially distributed windflow model run at 10 m resolution for eight windflow directions to produce maps of normalized wind speed values relative to the SDL station (see Musselman et al., 2015). From the prevailing wind direction (southwest), point values for each of the three simulation locations were extracted and this normalized value was multiplied by the wind speed measured at the SDL station (Table 1). For precipitation, hourly data from the nearby University Camp SNOTEL site was interpolated to the elevation of the SDL catchment through an iterative manual procedure specific to each site to align simulated and observed snow depth and SWE on the date of maximum accumulation. First, measured hourly precipitation at the nearest SNOTEL site (450 m lower in elevation and 2 km east) was doubled. Second, a SUMMA parameter used to scale frozen precipitation to approximate the effect of wind scour and drifting was manually tuned to match the observed maximum snow depth and SWE at each site (see Table 1). The precipitation adjustment informed by snow depth observations bypassed the challenges of explicitly simulating complex wind scour and drift dynamics. By accurately resolving maximum snow accumulation, the experiment could focus on better representing melt season dynamics (Brauchli et al., 2017). The remaining variables were assumed to be spatially invariant over the 0.3 km² catchment. The model was run from October 1, 2018, to September 30, 2019.

303

283

284

285

286

287

288

289

290

291

292

293

294

295

296

297

298

299

300

301

302

[Insert Table 1]

304305

306

307

308

310

311

312

313

314

In SUMMA, the vertical flux, q (m s⁻¹), and storage, θ_w (-), of liquid water in snow is parameterized as gravity drainage, where the hydraulic conductivity of snow is expressed using the Brooks and Corey relation (Brooks & Corey, 1964):

$$q = k_{sat} \left(\frac{\theta_w - \theta_{res}}{\theta_{sat} - \theta_{res}} \right)^c$$
 Eq. (4)

where k_{sat} (m s⁻¹) is the saturated hydraulic conductivity of snow, θ_{sat} (-) is the porosity of snow, θ_{res} (-) is the irreducible liquid water in the snowpack, and c is an exponent related to the pore size distribution. In Eq. (4), $\theta_{res} = \phi_{tens}\theta_{sat}$, where the parameter ϕ_{tens} defines the fraction of pore space that must be filled before drainage can occur (Clark, Nijssen, Lundquist, Kavetski, Rupp, Woods, Freer, Gutmann, Wood, Gochis, et al., 2015).

A model sensitivity analysis was conducted in which nine different parameter sets were created by modifying k_{sat} , ϕ_{tens} , and c each with three values that span observational ranges reported in the literature (e.g. Yamaguchi et al., 2012; Domine et al., 2013; Leroux & Pomeroy, 2019). As summarized in Table 2, k_{sat} was specified as 0.0005, 0.005, and 0.05 m s⁻¹, ϕ_{tens} was specified as 0.01, 0.06 and 0.15, and c was specified as 1, 3 and 5. A graphical visualization of these 9 sets of parameters shows the hydraulic conductivity as a function of θ_w (Fig. 4). To explore the sensitivity of results to the number of snow layers, the parameter sensitivity experiment was repeated with the snow model set to represent a maximum of 5 and 100 snow layers. Thus, the nine parameter sets (Table 2) were run twice for a total of 18 simulations at each of three sites.

This modelling sensitivity analysis allowed a comparison of a 100-layer and 5-layer representations of snowpack stratigraphy that are commonly utilized in hydrologic models (e.g., SNTHRM and CLM, respectively; Jordan, 1991; Toure et al., 2016). Within this comparison, we then explored the sensitivity of modifying the parameters that govern liquid water storage and flux in Eq. 4 as described above. Thus, the SUMMA simulations allowed comparisons between hydrologic model decisions that are often part of the internal structure of hydrologic models.

[Insert Table 2]

[Insert Figure 4]

3. RESULTS

3.1 Observations

The 2019 snow season at the nearby University Camp SNOTEL site was close to the long-term median for observed SWE values (1981-2010; Fig. 5). The long-term median peak SWE is 483 mm occurring 2-May. In 2019, peak SWE was 106% of the median (513 mm) and occurred 10-days later, on 12-May. After peak SWE, snowmelt progressed relatively consistently except for two accumulation events in late-May and late-June. Snow depth in the SDL catchment ranged from zero in wind-scoured areas up to nearly 7 m in drifts with peak d_s during the May 23rd survey (Table 3). The observation-based snow θ_w was highly variable, with values ranging from near zero to \geq 0.3 (Fig. 6, Table 4).

[Insert Figure 5]

350 [Insert Table 3]

352 [Insert Table 4]

Locations that had particularly high θ_w include shallow snow near the base of a hillslope in flat terrain and on a south aspect hillslope near the edges of large drifts (Fig. 6). These locations had consistently higher θ_w throughout the observation period. Generally, over the observation period, θ_w increased in value and variability (Table 4). Lower θ_w values were observed in the first two weeks after peak d_s with mean values close to 0.14. Beyond two weeks from peak d_s , θ_w increased with a maximum mean value of 0.18 occurring on 20-June. The increases in θ_w generally corresponded with increases in streamflow and similarly, decreases in θ_w coincided with decreases in streamflow (Fig. 7a). Decreases in θ_w typically coincided with snow accumulation events during which active melt paused and cold, dry snow accumulated. These snow accumulation events, and associated decreases in θ_w , were observed prior to the 23-May and 26-Jun surveys.

[Insert Figure 6]

[Insert Figure 7]

Regression analysis of our observations show that snow depth is strongly correlated with θ_w in a non-linear fashion with a r^2 value of 0.62 (3rd-order polynomial; Fig. 8, Table 5). A similar regression of θ_w with distance to bare soil resulted in an r^2 value of 0.32 (Fig. 8, Table 5). Both regressions were significant at the 0.01 level. Other parameters investigated for correlation to θ_w include slope, aspect, elevation, and terrain curvature, though none of these parameters resulted in r^2 values greater than 0.30 when considered individually. When considering multiple parameters, combining snow depth and distance to bare soil achieved an r^2 value of 0.67 and combining snow depth with ground surface slope resulted in an r^2 value of 0.65, both significant at the 0.01 level. For all regressions, best fits were achieved with third order polynomial regressions, highlighting the strong non-linearity of θ_w with these terrain and snow depth variables (Fig. 8, Table 5).

Additionally, a local-scale grid was repeatedly surveyed near the base of a hillslope where the terrain transitions to a flat slope. This grid was the same location as the plot-scale

study conducted in 2017 by Webb et al. (2020). Spatial patterns in the distribution of θ_w at the local-scale hold throughout the observation period and result in a similar distribution of θ_w as observed in 2017 (Webb et al., 2020), suggesting that this is not an anomalous year or set of observations, but rather indicative of the distribution of θ_w within the snowpack during the melt season for the SDL catchment. This plot contains some of the highest variability in θ_w observed within the SDL catchment, with high values consistently observed in the flat terrain throughout the observation period. Because of this high variability and previous plot-scale studies at this location, this was one of our simulated sites for the modelling portion of this investigation (Site 1).

[Insert Figure 8]

[Insert Table 5]

3.2 Modelling

Sites 1, 2, and 3 had observed maximum snow depths of 200 cm, 320 cm, and 450 cm, respectively. Despite being tuned to closely match the observed site-dependent effects of wind scour and drifting on seasonal maximum snow depth and SWE via modification of the frozen precipitation multiplier (Table 1), the ensemble spread of 18 SUMMA simulations at three sites did not uniformly correspond with observed θ_w . Nor was θ_w at the three sites simply explained by variations in snowpack depth or SWE. Fig. 9 shows the observed and modelled snow depth, SWE, and θ_w at the three sites during the observation campaign. Perturbing the three parameters governing snowpack liquid water transmission and storage, as well as the maximum number of snow layers, had the greatest effect on θ_w , followed by SWE, and the least effect on d_s (Fig. 9; inferred from the modelled range of each variable indicated by the grey shading).

[Insert Figure 9]

SUMMA generally did not simulate substantial inter-site variability in LWC. Simulated θ_w generally increased from near-zero in mid-May to reach a plateau in early-June that persisted through the melt season. Simulated θ_w generally did not exceed 0.2 and the magnitude was sensitive to the parameter values in Eq. 4. In contrast, the observed θ_w magnitude varied greatly among sites yet exhibited a similar seasonal increase in May and

plateau in June. Site 1 had the highest observed mean and standard deviation of θ_w of the three sites despite having the shallowest snowpack and the slowest seasonal melt rate (inferred from the slope of a line fit to the SWE observations in Fig. 9d; not shown). Of the three sites, the simulations at Site 1 had the largest mean absolute error (MAE) in θ_w , followed by Site 3 and the lowest errors occurred at Site 2 (Fig. 10). Indeed, SUMMA accurately simulated depth, SWE, and θ_w at Site 2.

No single parameter set universally minimized the θ_w error (Fig. 10). Generally, simulations with lowest k_{sat} and highest c (related to pore size distribution and thus indirectly related to grain size) values performed best (simulation IDs 1 and 2; Fig. 10 and Table 2). At Site 2, where simulated θ_w errors were smallest, the simulation with the highest k_{sat} and highest c values performed best (simulation ID 6) and the same simulation was ranked third-best at the other two sites (Fig. 10). With only one exception (Site 2; simulation ID 2), the five-layer snow model outperformed the 100-layer snow model in estimating LWC compared to observations.

[Insert Figure 10]

4. DISCUSSION

We present a unique observation campaign of snow θ_w at the slope to watershed scale. Using lidar and GPR measurements, the estimated θ_w values ranged from what would be expected to higher than previously documented in any study, to our knowledge. We observed the highest variability of liquid water storage in the snowpack near the base of a hillslope in flat terrain and on sloped terrain at the edges of deep snow drifts. A previous study in the SDL catchment using hydrogeochemical end member mixing analysis concluded that ~60% of the annual streamflow is a result of overland or lateral within-snow flow paths and ~10% interflow (Hill, 2017). This has been explained by a combination of frozen ground that inhibits infiltration in the winter and spring (Rey, Hinckley, Walvoord, & Singha, 2021; M. Williams et al., 2015) and saturation excess overland flow as the deep snow produces snowmelt volumes above the storage capacity of the relatively shallow soils (Hill, 2017). Our observations confirm that high θ_w interpreted to mean ponding at the snow-soil interface is occurring within the snowpack that is likely producing overland/intra-snowpack flow. Importantly, our observations bring new insight to the catchment-scale distribution of these processes. Rather than elevated θ_w occurring across a widespread area, our results suggest that regions of very high θ_w values (i.e., > 0.2) are highly localized at the base of a hillslope

and shallow snow adjacent to deeper snowdrifts (Fig. 6) yet may contribute disproportionately to catchment response (Fig. 7). Future efforts to further detail and predict where these processes are occurring will promote the improvement of conceptual models of physical hydrologic flow paths that occur during the spring snowmelt season in headwater basins (Fig. 11).

[Insert Figure 11]

The strong correlation of high θ_w and shallow snow depth (Fig. 8) is consistent with a similar relation previously observed at the point scale from lysimeters measuring snowmelt at a treeline site (Webb, Williams, et al., 2018). In the present study of an alpine catchment, the ponding of meltwater at the snow-soil interface may also be the result of the of the nearsurface water table rising into the snowpack as meltwater is transported to localized areas faster than it can be conveyed elsewhere (Fig. 11). This is likely the result of snowmelt being transported readily along a combination of interflow and inter-snowpack flow paths with high hydraulic conductivities (Webb et al., 2021; Webb et al., 2020). Furthermore, these observations of high θ_w in localized areas are similar to those in previous years at the plot scale (Rikkers, Williams, & Sommerfeld, 1996) and SDL catchment scale (Webb et al., 2020) suggesting that this process of accumulating meltwater at the snow-soil interface is regularly occurring during each melt season. While frozen soils have been previously posed as a hypothesis in playing a role in infiltration processes in the SDL catchment, our observations do not provide conclusive evidence to this effect. Frozen soil has been shown to increase interflow processes within the SDL catchment on hillslopes at lower elevations and with a less spatially continuous snowpack (Rey et al., 2021). However, the proximity of high θ_w values to bare soil, that would have lacked insulation from cold air temperatures, suggests that frozen soil may be a topic to investigate further in future studies.

The SUMMA model was able to adequately capture the melt season progression of snow depth and SWE at multiple sites after the date of peak accumulation, suggesting that the model was accurately resolving snowmelt rates via the calculation of snow mass and energy budgets. As for θ_w , the simulations show reasonable results for site 2, but underestimated values at Sites 1 and 3 (Figs. 9 & 10). The observed θ_w at Site 3 was within the range of simulated θ_w for ~50% of the surveys whereas Site 1 observed θ_w was always well above the simulated values (Fig. 9). Algorithms and parameter ranges used to simulate liquid water storage and transmission are developed and tested at point-scales that lack the terrain and

snowpack complexities examined in the present study. Additionally, no hydrologic model, to our knowledge, allows for the lateral flow of liquid water through snow that has been shown to occur within the SDL catchment (Rikkers et al., 1996; Webb et al., 2021; Webb et al., 2020). Most hydrologic models only allow for lateral water transport after meltwater is released from the snowpack (Fig. 1). However, even if surface runoff beneath a snowpack is simulated to occur, it is routed as surface flow that lacks the porous media physics that occur within a snowpack. A lack of connection between the snowpack and ground surface in hydrologic model structure results in water storage processes that occur in our catchment to be neglected in model simulations. Thus, we present a conceptual model of the physical processes (Fig. 11) and how these may be incorporated into simulations for SDL during snowmelt that includes variably saturated flow paths within the snowpack to create lateral connectivity above the snow-soil interface as variably saturated porous media flow (Fig. 12).

[Insert Figure 12]

Intra-snowpack lateral connectivity has been shown to occur during rain-on-snow and regular seasonal snowmelt events (e.g. Eiriksson et al., 2013; Würzer, Jonas, Wever, & Lehning, 2016; Webb et al., 2020). Hydraulic barriers that include both capillary and permeability barriers have been shown to laterally divert liquid water tens of meters within a snowpack (Eiriksson et al., 2013) with simulations suggesting orders of magnitude differences in hydrologic fluxes (Webb et al., 2021; Webb, Fassnacht, Gooseff, et al., 2018). These diversions have also been observed to result in locations of focused infiltration at rates that are high enough to produce infiltration excess runoff (Webb, Williams, et al., 2018). When multiple flow paths converge, liquid water can accumulate faster than the snowpack and soil can transport the water elsewhere resulting in the rising of the local water table above the snow-soil interface and into the snowpack as observed in SDL as well as elsewhere (Webb, Fassnacht, & Gooseff, 2018). These above-described processes result in spatially and temporally dynamic flow paths that impact the hydrologic connectivity of a headwater catchment (Fig. 11) with increased streamflow during days of higher liquid water retention in snow (Fig. 7).

Further investigations could be conducted to address some of the limitations in the current study. Our observation campaign would benefit from detailed soil moisture observations to further determine the saturation level of the soil beneath the snow. Soil moisture and temperature sensors could be installed strategically based upon the results of the

presented work to capture the variability of within-snow liquid water storage and basal ice lenses near the snow-soil interface. The surveyed transects could also be further refined to better capture the variability in snow depths and further test the presented regressions (Table 5). Lastly, we did not compare SUMMA modelled snowmelt rates to infiltration capacities of the soils within the SDL catchment that can vary widely amongst soil types and soil ice content (Hermes, 2019; Hermes et al., 2020). Combining observations that address the limitations of the present study could further elucidate runoff processes and flow paths occurring within an alpine catchment beneath the snowpack during the spring melt season. Future research is necessary to determine the significance of these processes in streamflow generation.

We recommend that future studies explore the importance of lateral flow through snow in sloped terrain by incorporating intra-snowpack lateral connectivity in hydrologic models (Fig. 12) and investigations to determine the frequency of surface runoff in the presence of a snowpack. Previous work has shown that these processes are likely less important at lower elevation, forested sites (Thayer et al., 2018; Webb et al., 2020). However, further studies are necessary to determine the controlling factors that determine the significance, or lack thereof, of intra-snowpack flow paths and the role that they play in runoff production.

5. CONCLUSIONS

We present a detailed observation campaign of snow depth and snow LWC at the watershed scale using terrestrial scanning lidar and surveys of ground penetrating radar. The results show high spatial variability of liquid water in an alpine snowpack during the spring snowmelt season. Statistical analyses show that volumetric liquid water content is most highly correlated to snow depth ($r^2 = 0.62$), with higher liquid water storage occurring in locations of shallow snow at the base of a hillslope and adjacent to deeper snow patches. Including the distance to bare soil and topographical slope slightly improved the coefficient of determination ($r^2 = 0.67$). We observed an area of the alpine basin that consistently had high volumetric liquid water content at the base of a hillslope throughout the snowmelt season. However, throughout the entire observation campaign, regions with high volumetric liquid water content values remained consistently high throughout the melt season. We present a conceptual model of the physical runoff processes that have been previously shown in our alpine catchment and how they converge to produce the spatial patterns observed in the present study. While hydrologic models have the flexibility to simulate many of the observed

dynamics in snowpack liquid water storage, model simulations using previously published parameter ranges underestimated the high liquid water storage at one of the three sites. This is a result of current model structures that lack capabilities for surface ponding of water within a snowpack or lateral flow through a snowpack. The results of the present study improve process-level understanding of physical hydrologic processes during snowmelt. This understanding may be used to improve hydrologic models to better simulate the interactions amongst snow distribution, melt, ET, and runoff. **ACKNOWLEDGEMENTS** We would like to acknowledge the contributions of the staff at the Niwot Ridge Long Term Ecological Research site and the Boulder Creek Critical Zone Observatory. This work was supported by the National Science Foundation award 1824152, the Niwot Ridge LTER cooperative agreement number DEB-1637686, and Boulder Creek CZO cooperative agreement number EAR-1331828. DATA AVAILABILITY Terrestrial lidar scan data are available through UNAVCO (https://tls.unavco.org/projects/U-072/) and the airborne lidar data used for model parameterization are available through the Niwot Ridge LTER repository (https://doi.org/10.6073/pasta/458c3932f7786b1da02a9c900baf594b). Saddle Catchment meteorological station data can be found through the Niwot Ridge LTER repository (https://portal.edirepository.org/nis/mapbrowse?packageid=knb-lter-nwt.168.2). Saddle Catchment ultrasonic snow depth data can be found through the Niwot Ridge LTER repository (https://doi.org/10.6073/pasta/c1a7a58e355112c362d35092071fa1f0). University Camp SNOTEL station data can be found through USDA publicly available data (https://wcc.sc.egov.usda.gov/nwcc/site?sitenum=838). REFERENCES Anderson, S.P., Guo, Q., and Parrish, E. (2013). Snow-Off Digital Terrain Model (DTM)

553

554

555

556

557

558

559

560

561

562

563

564

565

566

567

568

569

570

571

572

573

574

575

576

577

578

579

580

581

582

583

584

585

from 2010 LiDAR for the Boulder Creek Critical Zone Observatory (CZO), Colorado

586	ver 1. Environmental Data Initiative.
587	https://doi.org/10.6073/pasta/458c3932f7786b1da02a9c900baf594b
588	Bales, R. C., Molotch, N. P., Painter, T. H., Dettinger, M. D., Rice, R., & Dozier, J. (2006).
589	Mountain hydrology of the western United States. Water Resources Research, 42(8),
590	W08432. doi:10.1029/2005wr004387
591	Barnett, T. P., Adam, J. C., & Lettenmaier, D. P. (2005). Potential impacts of a warming
592	climate on water availability in snow-dominated regions. Nature, 438(7066), 303-309.
593	doi:10.1038/nature04141
594	Barnhart, T., Molotch, N., Livneh, B., Harpold, A., Knowles, J., & Schneider, D. (2016).
595	Snowmelt rate dictates streamflow. Geophysical Research Letters, 43(15), 8006-8016.
596	doi:10.1002/2016GL069690
597	Bracken, L., & Croke, J. (2007). The concept of hydrological connectivity and its
598	contribution to understanding runoff-dominated geomorphic systems. Hydrological
599	Processes, 21(13), 1749-1763. doi:10.1002/hyp.6313
600	Bradford, J., Harper, J., & Brown, J. (2009). Complex dielectric permittivity measurements
601	from ground-penetrating radar data to estimate snow liquid water content in the
602	pendular regime. Water Resources Research, 45. doi:10.1029/2008WR007341
603	Brauchli, T., Trujillo, E., Huwald, H., & Lehning, M. (2017). Influence of Slope-Scale
604	Snowmelt on Catchment Response Simulated With the Alpine3D Model. Water
605	Resources Research, 53(12), 10723-10739. doi:10.1002/2017WR021278
606	Brooks, R. H., & Corey, A. T. (1964). Hydraulic Properties of Porous Media. Retrieved from
607	Fort Collins, CO:
608	Clark, M., Fan, Y., Lawrence, D., Adam, J., Bolster, D., Gochis, D., Zeng, X. (2015).
609	Improving the representation of hydrologic processes in Earth System Models. Water
610	Resources Research, 51(8), 5929-5956. doi:10.1002/2015WR017096
611	Clark, M., Nijssen, B., & Luce, C. (2017). An analytical test case for snow models. Water
612	Resources Research, 53(1), 909-922. doi:10.1002/2016WR019672
613	Clark, M., Nijssen, B., Lundquist, J., Kavetski, D., Rupp, D., Woods, R., Rasmussen, R.
614	(2015). A unified approach for process-based hydrologic modeling: 1. Modeling
615	concept. Water Resources Research, 51(4), 2498-2514. doi:10.1002/2015WR017198
616	Clark, M., Nijssen, B., Lundquist, J., Kavetski, D., Rupp, D., Woods, R., Marks, D.
617	(2015). A unified approach for process-based hydrologic modeling: 2. Model
618	implementation and case studies. Water Resources Research, 51(4), 2515-2542.
619	doi:10.1002/2015WR017200

- 620 Colbeck, S. C. (1991). The layered character of snow covers. Reviews of Geophysics, 29(1),
- 621 81-96.
- Deems, J., Painter, T., & Finnegan, D. (2013). Lidar measurement of snow depth: a review.
- Journal of Glaciology, 59(215), 467-479. doi:10.3189/2013JoG12J154
- Detty, J., & McGuire, K. (2010). Threshold changes in storm runoff generation at a till-
- mantled headwater catchment. Water Resources Research, 46.
- doi:10.1029/2009WR008102
- Domine, F., Morin, S., Brun, E., Lafaysse, M., & Carmagnola, C. M. (2013). Seasonal
- evolution of snow permeability under equi-temperature and temperature-gradient
- 629 conditions. The Cryosphere, 7(6), 1915-1929. doi:10.5194/tc-7-1915-2013
- 630 Eiriksson, D., Whitson, M., Luce, C. H., Marshall, H. P., Bradford, J., Benner, S. G., . . .
- McNamara, J. P. (2013). An evaluation of the hydrologic relevance of lateral flow in
- snow at hillslope and catchment scales. Hydrological Processes, 27(5), 640-654.
- 633 doi:10.1002/hyp.9666
- Elder, K., Dozier, J., & Michaelsen, J. (1991). Snow Accumulation and Distribution in an
- Alpine Watershed. Water Resources Research, 27(7), 1541-1552.
- Evans, S. G., Ge, S., Voss, C. I., & Molotch, N. P. (2018). The Role of Frozen Soil in
- 637 Groundwater Discharge Predictions for Warming Alpine Watersheds. Water
- Resources Research, 54(3), 1599-1615. doi:https://doi.org/10.1002/2017WR022098
- 639 Ford, C., Kendall, A., & Hyndman, D. (2020). Effects of shifting snowmelt regimes on the
- 640 hydrology of non-alpine temperate landscapes. Journal of Hydrology, 590.
- doi:10.1016/j.jhydrol.2020.125517
- Gasemizade, M., & Schirmer, M. (2013). Subsurface flow contribution in the hydrological
- cycle: lessons learned and challenges ahead-a review. Environmental Earth Science,
- 644 69, 707-718. doi:10.1007/s12665-013-2329-8
- 645 Harpold, A. A., Molotch, N. P., Musselman, K. N., Bales, R. C., Kirchner, P. B., Litvak, M.,
- & Brooks, P. D. (2015). Soil moisture response to snowmelt timing in mixed-conifer
- subalpine forests. Hydrological Processes, 29(12), 2782-2798. doi:10.1002/hyp.10400
- Heilig, A., Mitterer, C., Schmid, L., Wever, N., Schweizer, J., Marshall, H. P., & Eisen, O.
- 649 (2015). Seasonal and diurnal cycles of liquid water in snow-Measurements and
- modeling. Journal of Geophysical Research: Earth Surface, 120(10), 2139-2154.
- doi:10.1002/2015JF003593
- Hermes, A. (2019). Saturated and unsaturated hydraulic conductivity for Saddle Stream
- Network, 2017 ver 1. Environmental Data Initiative.

https://doi.org/10.6073/pasta/051f552fdaf1428df60ddeb72a7d184c (Accessed 2022-654 01-31). 655 Hermes A. L., Wainwright H. M., Wigmore O., Falco N., Molotch N. P., & Hinckley E. L.S. 656 (2020). From Patch to Catchment: A Statistical Framework to Identify and Map Soil 657 Moisture Patterns Across Complex Alpine Terrain. Front. Water 2:578602. doi: 658 10.3389/frwa.2020.578602. 659 Hill, A. F. (2017). Rapid Assessment of Hydrologic Controls on Mountain Water Resources. 660 (Doctoral Dissertation Dissertation), University of Colorado Boulder, Available from 661 662 CU Boulder CU Scholar database. Hirashima, H., Avanzi, F., & Wever, N. (2019). Wet-Snow Metamorphism Drives the 663 Transition From Preferential to Matrix Flow in Snow. Geophysical Research Letters, 664 46(24), 14548-14557. doi:10.1029/2019gl084152 665 Holbrook, W., Miller, S., & Provart, M. (2016). Estimating snow water equivalent over long 666 mountain transects using snowmobile-mounted ground-penetrating radar. Geophysics, 667 81(1), WA183-WA193. doi:10.1190/GEO2015-0121.1 668 669 Jencso, K., McGlynn, B., Gooseff, M., Wondzell, S., Bencala, K., & Marshall, L. (2009). Hydrologic connectivity between landscapes and streams: Transferring reach-and 670 671 plot-scale understanding to the catchment scale. Water Resources Research, 45, W04428. doi:10.1029/2008WR007225 672 Jencso, K. G., & McGlynn, B. L. (2011). Hierarchical controls on runoff generation: 673 Topographically driven hydrologic connectivity, geology, and vegetation. Water 674 Resources Research, 47, W11527. doi:10.1029/2011wr010666 675 Jennings, K., Kittel, T., Molotch, N., & Yang, K. (2021). Infilled climate data for C1, Saddle, 676 and D1, 1990 - 2019, hourly. ver 2. Environmental Data Initiative. 677 https://doi.org/10.6073/pasta/0bf785f2f77c3f558f633853a4465404 678 Jordan, R. (1991), A one-dimensional temperature model for a snow cover: Technical 679 documentation for SNTHERM 89, CRREL Rep. SR-91-16, Cold Reg. Res. and Eng. 680 Lab., Hanover, N. H. 681 Kampf, S., Markus, J., Heath, J., & Moore, C. (2015). Snowmelt runoff and soil moisture 682 dynamics on steep subalpine hillslopes. Hydrological Processes, 29(5), 712-723. 683 doi:10.1002/hyp.10179 684 Knowles, J., Harpold, A., Cowie, R., Zeliff, M., Barnard, H., Burns, S., . . . Williams, M. 685

(2015). The relative contributions of alpine and subalpine ecosystems to the water

balance of a mountainous, headwater catchment. Hydrological Processes, 29(22), 687 4794-4808. doi:10.1002/hyp.10526 688 Knowles, N., Dettinger, M., & Cayan, D. (2006). Trends in snowfall versus rainfall in the 689 Western United States. Journal of Climate, 19(18), 4545-4559. 690 doi:10.1175/JCLI3850.1 691 Koch, F., Prasch, M., Schmid, L., Schweizer, J., & Mauser, W. (2014). Measuring Snow 692 Liquid Water Content with Low-Cost GPS Receivers. Sensors, 14(11), 20975-20999. 693 doi:10.3390/s141120975 694 695 Kormos, P., Marks, D., McNamara, J., Marshall, H., Winstral, A., & Flores, A. (2014). Snow distribution, melt and surface water inputs to the soil in the mountain rain-snow 696 transition zone. Journal of Hydrology, 519, 190-204. 697 doi:10.1016/j.jhydrol.2014.06.051 698 Leroux, N. R., & Pomeroy, J. W. (2019). Simulation of capillary pressure overshoot in snow 699 combining trapping of the wetting phase with a nonequilibrium Richards equation 700 model. Water Resources Research, 55(1), 236-248. 701 702 https://doi.org/10.1029/2018WR022969 Leroux, N. R., Marsh, C. B., & Pomeroy, J. W. (2020). Simulation of preferential flow in 703 snow with a 2-D non-equilibrium Richards model and evaluation against laboratory 704 data. Water Resources Research, 56, e2020WR027466. 705 https://doi.org/10.1029/2020WR027466 706 Li, D., Wrzesien, M., Durand, M., Adam, J., & Lettenmaier, D. (2017). How much runoff 707 originates as snow in the western United States, and how will that change in the 708 future? Geophysical Research Letters, 44(12), 6163-6172. 709 doi:10.1002/2017GL073551 710 Liu, F., Williams, M. W., & Caine, N. (2004). Source waters and flow paths in an alpine 711 catchment, Colorado Front Range, United States. Water Resources Research, 40, 712 W09401. doi:10.1029/2004wr003076 713 López-Moreno, J. I., Fassnacht, S. R., Beguería, S., & Latron, J. B. P. (2011). Variability of 714 715 snow depth at the plot scale: implications for mean depth estimation and sampling strategies. The Cryosphere, 5(3), 617-629. doi:10.5194/tc-5-617-2011 716 Marshall, H., Koh, G., & Forster, R. (2005). Estimating alpine snowpack properties using 717 FMCW radar. Annals of Glaciology, 40, 157-162. doi:10.3189/172756405781813500 718

- McGlynn, B., & McDonnell, J. (2003). Quantifying the relative contributions of riparian and
- hillslope zones to catchment runoff. Water Resources Research, 39(11).
- 721 doi:10.1029/2003WR002091
- McNamara, J. P., Chandler, D., Seyfried, M., & Achet, S. (2005). Soil moisture states, lateral
- flow, and streamflow generation in a semi-arid, snowmelt-driven catchment.
- Hydrological Processes, 19(20), 4023-4038. doi:10.1002/hyp.5869
- 725 Mitterer, C., Heilig, A., Schweizer, J., & Eisen, O. (2011). Upward-looking ground-
- 726 penetrating radar for measuring wet-snow properties. Cold Regions Science and
- 727 Technology, 69(2-3), 129-138. doi:10.1016/j.coldregions.2011.06.003
- Molotch, N., Colee, M., Bales, R., & Dozier, J. (2005). Estimating the spatial distribution of
- snow water equivalent in an alpine basin using binary regression tree models: the
- 730 impact of digital elevation data and independent variable selection. Hydrological
- 731 Processes, 19(7), 1459-1479. doi:10.1002/hyp.5586
- Morse, J. and Niwot Ridge LTER. (2021). Saddle catchment sensor network data, 2017-
- 733 2020. ver 3. Environmental Data Initiative.
- 734 https://doi.org/10.6073/pasta/c1a7a58e355112c362d35092071fa1f0
- 735 Musselman, K., Addor, N., Vano, J., & Molotch, N. (2021). Winter melt trends portend
- widespread declines in snow water resources. Nature Climate Change, 11(5), 418-+.
- 737 doi:10.1038/s41558-021-01014-9
- Musselman, K., Clark, M., Liu, C., Ikeda, K., & Rasmussen, R. (2017). Slower snowmelt in a
- warmer world. Nature Climate Change, 7(3), 214-+. doi:10.1038/NCLIMATE3225
- Musselman, K., Lehner, F., Ikeda, K., Clark, M., Prein, A., Liu, C., ... Rasmussen, R.
- 741 (2018). Projected increases and shifts in rain-on-snow flood risk over western North
- America. Nature Climate Change, 8(9), 808-+. doi:10.1038/s41558-018-0236-4
- Musselman, K. N., Molotch, N. P., & Margulis, S. A. (2017). Snowmelt response to
- simulated warming across a large elevation gradient, southern Sierra Nevada,
- 745 California. The Cryosphere, 11(6), 2847-2866. doi:10.5194/tc-11-2847-2017
- Peitzsch, E., Birkeland, K. W., & Hansen, K. J. (2008). Water movement and capillary
- barriers in a stratified and inclined snowpack. Paper presented at the International
- 748 Snow Science Workshop, Whistler.
- Rey, D. M., Hinckley, E.-L. S., Walvoord, M. A., & Singha, K. (2021). Integrating
- observations and models to determine the effect of seasonally frozen ground on
- hydrologic partitioning in alpine hillslopes in the Colorado Rocky Mountains, USA.
- 752 Hydrological Processes, 35(10), e14374. doi:https://doi.org/10.1002/hyp.14374

- Rikkers, M., Williams, M. W., & Sommerfeld, R. A. (1996). Spatial variance of snowmelt at
- a continental alpine site Paper presented at the Western Snow Conference, 64th
- 755 Annual Meeting, Bend, Oregon.
- Roth, K., SCHULIN, R., FLUHLER, H., & ATTINGER, W. (1990). Calibration of time
- domain reflectometry for water-content measurement using a composite dielectric
- 758 approach. Water Resources Research, 26(10), 2267-2273.
- 759 doi:10.1029/WR026i010p02267
- Schmid, L., Koch, F., Heilig, A., Prasch, M., Eisen, O., Mauser, W., & Schweizer, J. (2015).
- A novel sensor combination (upGPR-GPS) to continuously and nondestructively
- derive snow cover properties. Geophysical Research Letters, 42(9), 3397-3405.
- 763 doi:10.1002/2015GL063732
- Schmucki, E., Marty, C., Fierz, C., & Lehning, M. (2014). Evaluation of modelled snow
- depth and snow water equivalent at three contrasting sites in Switzerland using
- SNOWPACK simulations driven by different meteorological data input. Cold
- Regions Science and Technology, 99, 27-37. doi:10.1016/j.coldregions.2013.12.004
- Sexstone, G. A., & Fassnacht, S. R. (2014). What drives basin scale spatial variability of
- snowpack properties in northern Colorado? The Cryosphere, 8(2), 329-344.
- 770 doi:10.5194/tc-8-329-2014
- 771 Stewart, I., Cayan, D., & Dettinger, M. (2004). Changes in snowmelt runoff timing in
- western North America under a 'business as usual' climate change scenario. Climatic
- 773 Change, 62(1-3), 217-232. doi:10.1023/B:CLIM.0000013702.22656.e8
- Thayer, D., Parsekian, A., Hyde, K., Speckman, H., Beverly, D., Ewers, B., ... Holbrook, W.
- 775 (2018). Geophysical Measurements to Determine the Hydrologic Partitioning of
- Snowmelt on a Snow-Dominated Subalpine Hillslope. Water Resources Research,
- 54(6), 3788-3808. doi:10.1029/2017WR021324
- 778 Toure, A. M., Rodell, M., Yang, Z., Beaudoing, H., Kim, E., Zhang, Y., & Kwon, Y. (2016).
- Evaluation of the Snow Simulations from the Community Land Model, Version 4
- 780 (CLM4). Journal of Hydrometeorology, 17(1), 153–170.
- 781 https://doi.org/10.1175/JHM-D-14-0165.1
- Vano, J., Udall, B., Cayan, D., Overpeck, J., Brekke, L., Das, T., . . . Lettenmaier, D. (2014).
- Understanding Uncertainties in Future Colorado River Streamflow. Bulletin of the
- American Meteorological Society, 95(1), 59-78. doi:10.1175/BAMS-D-12-00228.1

Wada, Y., & Bierkens, M. (2014). Sustainability of global water use: past reconstruction and 785 future projections. Environmental Research Letters, 9(10). doi:10.1088/1748-786 9326/9/10/104003 787 Webb, R., Jennings, K., Finsterle, S., & Fassnacht, S. (2021). Two-dimensional liquid water 788 789 flow through snow at the plot scale in continental snowpacks: simulations and field data comparisons. Cryosphere, 15(3), 1423-1434. doi:10.5194/tc-15-1423-2021 790 791 Webb, R. W. (2017). Using ground penetrating radar to assess the variability of snow water equivalent and melt in a mixed canopy forest, Northern Colorado. Frontiers of Earth 792 793 Science, 11(3), 482-495. doi:10.1007/s11707-017-0645-0 Webb, R. W., Fassnacht, S. R., & Gooseff, M. N. (2015). Wetting and Drying Variability of 794 the Shallow Subsurface Beneath a Snowpack in California's Southern Sierra Nevada. 795 Vadose Zone Journal, 14(8). doi:10.2136/vzj2014.12.0182 796 Webb, R. W., Fassnacht, S. R., & Gooseff, M. N. (2018). Hydrologic flow path development 797 varies by aspect during spring snowmelt in complex subalpine terrain. Cryosphere, 798 799 12(1), 287-300. doi:10.5194/tc-12-287-2018 800 Webb, R. W., Fassnacht, S. R., Gooseff, M. N., & Webb, S. W. (2018). The Presence of Hydraulic Barriers in Layered Snowpacks: TOUGH2 Simulations and Estimated 801 802 Diversion Lengths. Transport in Porous Media, 123(3), 457-476. doi:10.1007/s11242-018-1079-1 803 Webb, R. W., Jennings, K., Fend, M., & Molotch, N. (2018). Combining Ground Penetrating 804 Radar with Terrestrial LiDAR Scanning to Estimate the Spatial Distribution of Liquid 805 806 Water Content in Seasonal Snowpacks. Water Resources Research, 54, 10339-10349. doi:10.1029/2018WR022680 807 Webb, R. W., Wigmore, O., Jennings, K., Fend, M., & Molotch, N. P. (2020). Hydrologic 808 connectivity at the hillslope scale through intra-snowpack flow paths during 809 snowmelt. Hydrological Processes, 34(7), 1616-1629. doi:10.1002/hyp.13686 810 Webb, R. W., Williams, M. W., & Erickson, T. A. (2018). The Spatial and Temporal 811 812 Variability of Meltwater Flow Paths: Insights From a Grid of Over 100 Snow Lysimeters. Water Resources Research, 54(2), 1146-1160. 813 doi:10.1002/2017WR020866 814 Wever, N., Fierz, C., Mitterer, C., Hirashima, H., & Lehning, M. (2014). Solving Richards 815

816

817

Equation for snow improves snowpack meltwater runoff estimations in detailed multi-

layer snowpack model. The Cryosphere, 8(1), 257-274. doi:10.5194/tc-8-257-2014

818	Wieder, W. R., Knowles, J. F., Blanken, P. D., Swenson, S. C., & Suding, K. N. (2017).							
819	Ecosystem function in complex mountain terrain: Combining models and long-term							
820	observations to advance process-based understanding. Journal of Geophysical							
821	Research: Biogeosciences, 122(4), 825-845.							
822	doi:https://doi.org/10.1002/2016JG003704							
823	Williams, M., Erickson, T., & Petrzelka, J. (2010). Visualizing meltwater flow through snow							
824	at the centimetre-to-metre scale using a snow guillotine. Hydrological Processes,							
825	24(15), 2098-2110. doi:10.1002/hyp.7630							
826	Williams, M., Hood, E., Molotch, N., Caine, N., Cowie, R., & Liu, F. (2015). The 'teflon							
827	basin' myth: hydrology and hydrochemistry of a seasonally snow-covered catchment.							
828	Plant Ecology & Diversity, 8(5-6), 639-661. doi:10.1080/17550874.2015.1123318							
829	Williams, M. W., Rikkers, M., & Pfeffer, W. T. (2000). Ice columns and frozen rills in a							
830	warm snowpack, Green Lakes Valley, Colorado, USA. Nordic Hydrology, 31(3), 169-							
831	186.							
832	Williams, M. W., Seibold, C., & Chowanski, K. (2009). Storage and release of solutes from a							
833	subalpine seasonal snowpack: soil and stream water response, Niwot Ridge,							
834	Colorado. Biogeochemistry, 95(1), 77-94. doi:10.1007/s10533-009-9288-x							
835	Winchell, T., Barnard, D., Monson, R., Burns, S., & Molotch, N. (2016). Earlier snowmelt							
836	reduces atmospheric carbon uptake in midlatitude subalpine forests. Geophysical							
837	Research Letters, 43(15), 8160-8168. doi:10.1002/2016GL069769							
838	Würzer, S., Jonas, T., Wever, N., & Lehning, M. (2016). Influence of Initial Snowpack							
839	Properties on Runoff Formation during Rain-on-Snow Events. Journal of							
840	Hydrometeorology, 17(6), 1801-1815. doi:10.1175/JHM-D-15-0181.1							
841	Yamaguchi, S., Watanabe, K., Katsushima, T., Sato, A., & Kumakura, T. (2012).							
842	Dependence of the water retention curve of snow on snow characteristics. Annals of							
843	Glaciology, 53(61), 6-12. doi:10.3189/2012AoG61A001							
844								
845	TABLES							
846								
847	Table 1. Site characteristics and parameters used in the SUMMA model.							
	Slope, Aspect, Windspeed Frozen precipitation							
	deg. deg. factor factor							

0.92

0.65

Site 1 0

Site 2	12	111	0.85	1.45
Site 3	14	156	0.85 0.50	1.85

Table 2. Parameter values used in the SUMMA sensitivity analysis. Parameters shown include hydraulic conductivity (k_{sat} , m s⁻¹), fraction of pore space that must be filled prior to drainage (ϕ_{tens}), and pore size distribution (c).

			Simulati	Simulation ID						
Variable	1	2	3	4	5	6	7	8	9	
k_{sat}	0.0005	0.0005	0.0005	0.0005	0.05	0.05	0.05	0.05	0.005	
ϕ_{tens}	0.01	0.08	0.01	0.08	0.01	0.08	0.01	0.08	0.05	
C	5	5	1	1	5	5	1	1	3	

Table 3. Summary statistics for all snow depth (d_s) DEMs based on lidar scans including maximum, mean, median, standard deviation (Std. Dev.) and coefficient of variation (CV).

Date (2019)	$\operatorname{Max} d_{s}(\mathbf{m})$	Mean d_s (m)	Median d_s (m)	Std. Dev. (m)	CV
14-May	5.99	1.18	1.60	1.17	0.99
17-May	5.76	0.55	1.69	0.99	1.80
23-May	6.76	0.59	1.75	1.04	1.76
27-May	6.16	0.57	1.74	1.02	1.79
31-May	6.33	0.57	1.74	1.03	1.81
07-Jun	5.99	0.53	1.46	0.93	1.75
14-Jun	5.15	0.42	0.99	0.74	1.76
20-Jun	4.71	0.30	0.79	0.63	2.10
26-Jun	6.00	0.30	1.01	0.66	2.20
27-Jun	6.00	0.30	1.01	0.66	2.20
	ı				

Table 4. Summary statistics for all snow depth and volumetric liquid water content (θ_w) estimates along surveyed transects including maximum, mean, median, standard deviation (Std. Dev.) and coefficient of variation (CV).

			Si	iow Dep	th (m)	Volumetric Liquid Water Content (-)				
Date	n	Max	Mean	Median	Std. Dev.	CV	Mean	Median	Std. Dev.	CV
17-May	1930	3.97	1.56	1.54	0.78	0.50	0.157	0.140	0.054	0.346
23-May	1023	6.57	2.34	2.19	0.96	0.41	0.136	0.126	0.050	0.367
27-May	857	6.06	2.41	2.23	0.92	0.38	0.135	0.129	0.045	0.331
31-May	896	6.21	2.41	2.24	0.88	0.37	0.132	0.125	0.045	0.341
07-Jun	595	5.70	2.03	1.84	1.09	0.54	0.163	0.149	0.056	0.342
14-Jun	1023	5.01	1.67	1.53	0.82	0.49	0.166	0.155	0.056	0.336
20-Jun	1016	4.27	1.37	1.25	0.77	0.56	0.178	0.161	0.065	0.367
26-Jun	1034	6.00	1.39	1.22	0.82	0.59	0.168	0.159	0.064	0.384
27-Jun	917	6.00	1.42	1.24	0.86	0.60	0.165	0.156	0.064	0.391
	1						1			

Table 5. Results of volumetric liquid water content regression analysis showing the parameters used, resulting r^2 , and fit equation. All regressions shown were found to be significant at the 0.01 level.

Parameters	r^2	Equation					
Snow Depth	0.62	$-0.005x^3 + 0.047x^2 - 0.167x + 0.316$					
Dist. to Bare Soil	0.32	$-2.32e^{-7}x^3 + 6.04e^{-5}x^2 - 0.005x + 0.254$					
Snow Depth (x)	0.67	$0.33 - 0.15x - 1.9e^{-3}y + 0.04x^2 + 3.3e^{-4}xy + 1.5e^{-5}y^2$					
Dist. to Bare Soil (y)	0.07	$-4.1e^{-3}x^3 + 3.9e^{-5}x^2y - 4.7e^{-6}xy^2$					
Snow Depth (x)		$0.36 - 0.16x - 0.01y + 0.04x^2 + 1.3e^{-3}xy + 5.4e^{-4}y^2$					
Ground Surface	0.65	$-4.5e^{-3}x^3 + 4.4e^{-4}x^2y - 1.3e^{-4}xy^2$					
Slope (y)		7.5c x 1 4.4c x y = 1.5c xy					

FIGURE LEGENDS 869 870 Figure 1. Visualizations of hydrologic model structure that is commonly applied when a 871 snowpack is present. Note the lack of lateral connectivity between two adjacent snowpacks. 872 873 Figure 2. Summary of the Saddle Catchment (SDL) physiographic characteristics including: 874 875 a) satellite imagery showing treeline, b) general location of SDL in the contiguous United States, c) elevation, d) topographic slope, and e) topographic aspect. 876 877 Figure 3. a) Lidar derived snow depth on 14-May 2019 used to determine b) the normalized 878 distribution of snow depth relative to the snow depth sensor (77 cm on 14-May). c) A 879 comparison to the SNOTEL station depth shows a linear correlation with an r² value of 0.89 880 during the melt season. No data were collected below tree line during the lidar scans as 881 882 indicated by the hashed area in panels a and b. 883 Figure 4. The hydraulic conductivity of snow as a function of volumetric liquid water 884 content (θ_w) using the 9 sets of parameters presented in Table 2. Note that the y-axis is 885 886 presented in log scale. 887 Figure 5. A comparison of the 2019 snow water equivalent (SWE) to the 30-year median 888 (1981-2010) at the University Camp SNOTEL station. 889 890 Figure 6. Observed snow depth and volumetric LWC for representative dates of a) early 891 snowmelt prior to observable runoff, b) moderate snowmelt during the rising limb of the 892 hydrograph, and c) peak snowmelt immediately prior to peak runoff. Insets indicated the 893 timing of each observation relative to the observed hydrograph at the SDL stream gage. For 894 895 visual purposes, LWC was resampled to a 10 m raster and LWC was only calculated along 896 GPR transects. 897 Figure 7. (a) Observed discharge at the SDL stream gauge and the percent of observed 898 snowpack volumetric LWC that was > 15%. (b) histogram of volumetric LWC observations 899 for 23-May and 27-June. 900

Figure 8. Third order polynomial regressions for (a) snow depth vs. θ_w , (b) distance to bare 902 soil vs θ_w , (c) snow depth and distance to bare soil vs. θ_w , and (d) snow depth and ground 903 surface slope vs. θ_w . The associated r² values are given for each regression and all regressions 904 are shown to a maximum θ_w of 0.3. 905 906 Figure 9. At each of the three study sites (panel columns), simulations and observations of 907 snow depth (a-c), snow water equivalent (d-f), and volumetric liquid water content (g-i). 908 Mean observations are indicated as a point with whiskers extending one standard deviation 909 910 calculated based on a 20 m by 20 m box centered on the modeled locations. Simulations are shown as the range (gray shading) of 18 parameter sensitivity runs. Three example 911 simulations (slow, moderate, and fast draining) are shown as the blue, black and red lines in 912 913 the bottom panels. 914 915 Figure 10. Mean absolute error in SUMMA simulations of volumetric liquid water content, cm cm⁻³, at each of the three sites (panel columns). Errors (y-axis) are ranked by simulation 916 917 ID (x-axis; ranking is lowest to highest, left to right) for the five-layer snow model (gray bars). The error accompanying the five-layer ranked simulation ID is also shown for the 100-918 919 layer snow model (blue bars). 920 Figure 11. Conceptual diagram showing the meltwater flow through-snow processes that 921 occur including: a) ponding water on ice lenses, b) saturation excess through-snow flow, c) 922 diversion of flow paths along stratigraphic layers (i.e. hydraulic barriers), d) lateral advancing 923 of a wetting front, and e) infiltration excess as a result of focused infiltration. 924 925 Figure 12. Visualizations of hydrologic model structure that is recommended for further 926 investigation based on the present study that adds connectivity between the snowpack and 927 soil and lateral connectivity within the snowpack above the snow-soil interface. Changes to 928 929 the structure from Figure 1 are indicated in red. 930 931 932 933 934

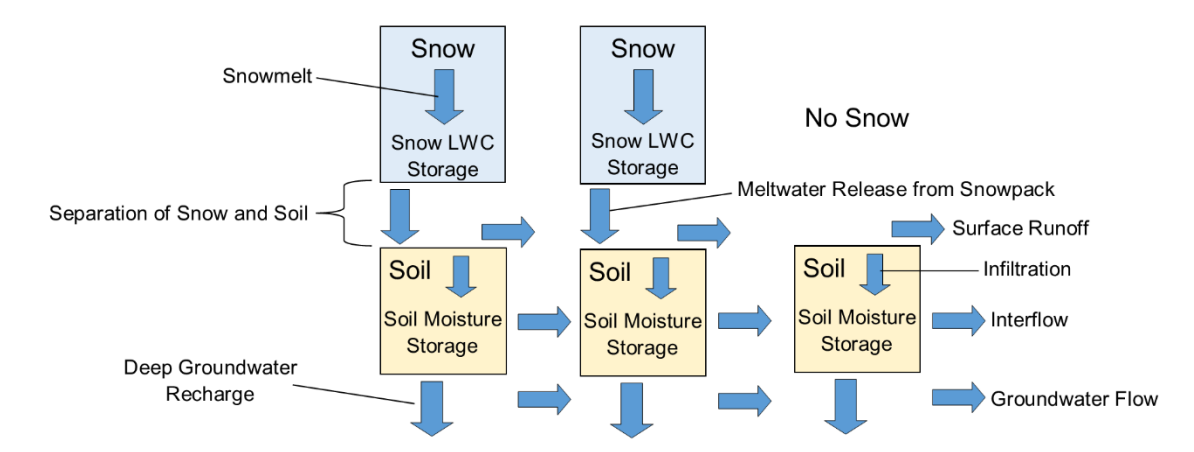


Figure 1. Visualizations of hydrologic model structure that is commonly applied when a snowpack is present on the ground surface. Note the lack of lateral connectivity between two adjacent snowpacks.

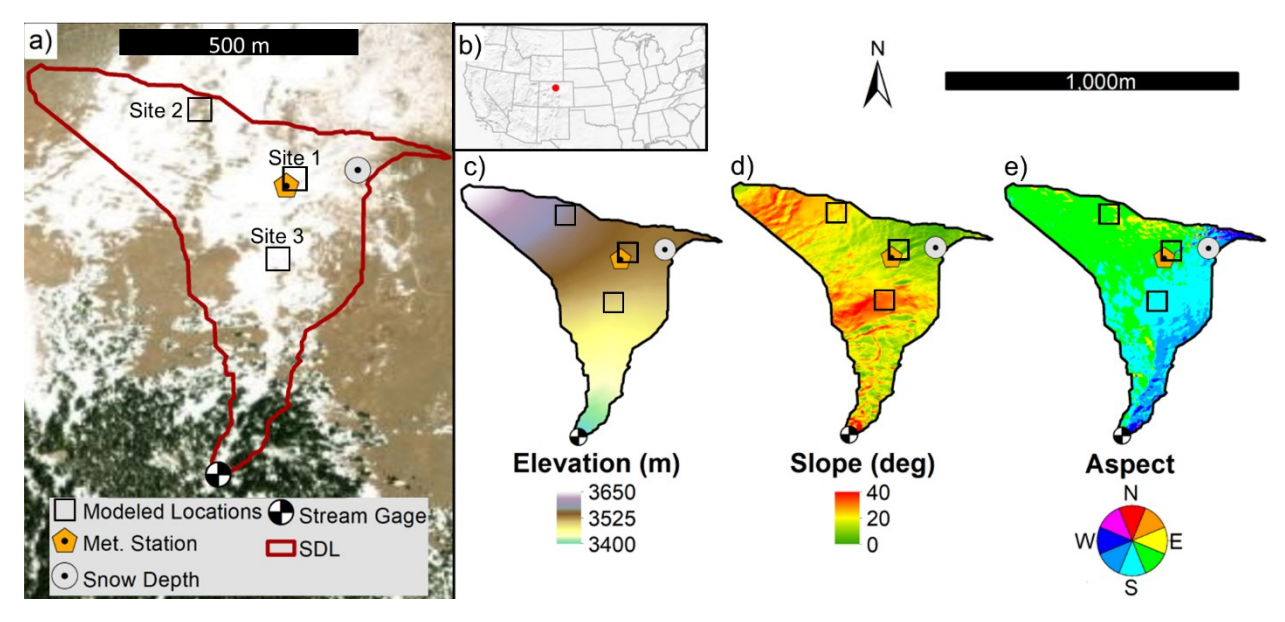


Figure 2. Summary of the Saddle Catchment (SDL) physiographic characteristics including: a) satellite imagery showing treeline, b) general location of SDL in the contiguous United States, c) elevation, d) topographic slope, and e) topographic aspect.

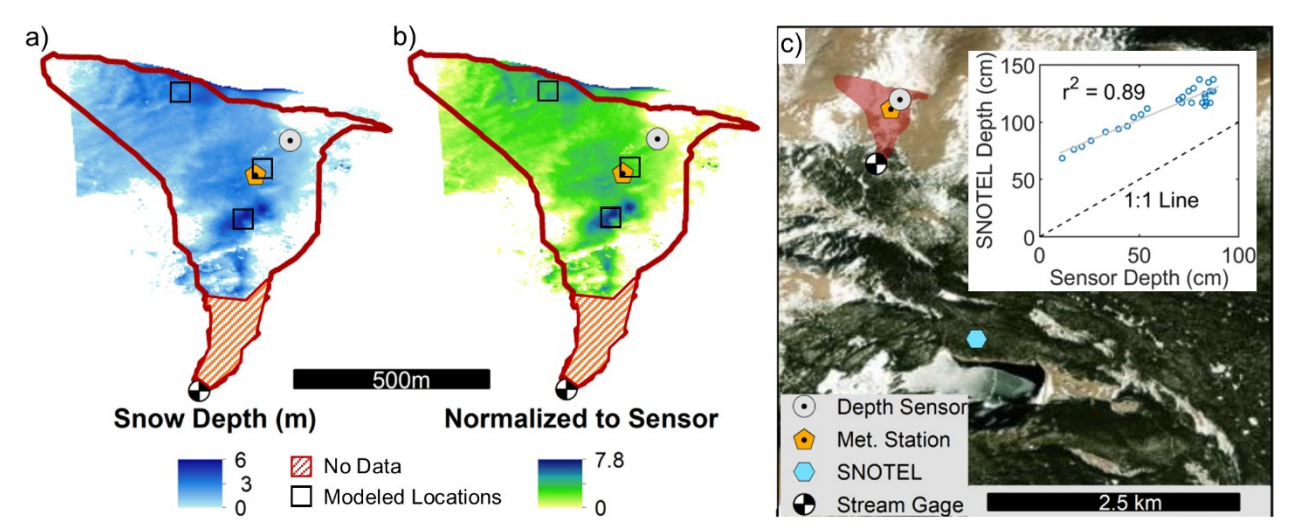


Figure 3. a) Lidar derived snow depth on May 14, 2019 used to determine b) the normalized distribution of snow depth relative to the snow depth sensor (77 cm on May 14). c) A comparison to the SNOTEL station depth shows a linear correlation with an r^2 value of 0.89 during the melt season. No data were collected below tree line during the Lidar scans as indicated by the hashed area in panels a and b.

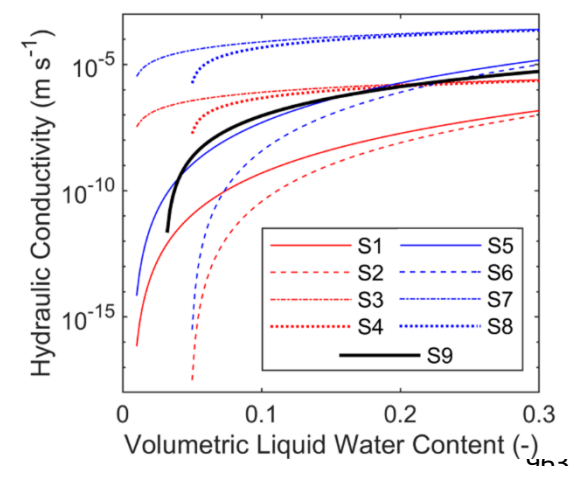


Figure 4. The hydraulic conductivity of snow as a function of volumetric water content (θ_w) using the 9 sets of parameters presented in Table 2. Parameter sets are organized by their simulation ID in Table 2. Note that the y-axis is presented in log scale.

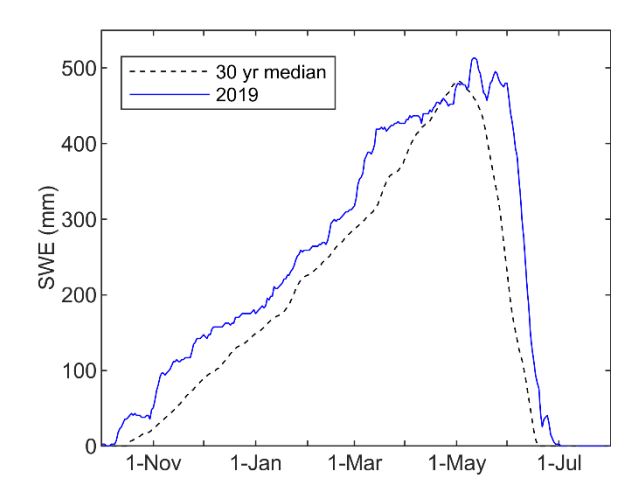


Figure 5. A comparison of the 2019 snow water equivalent (SWE) to the 30-year median (1981-2010) at the University Camp SNOTEL station.

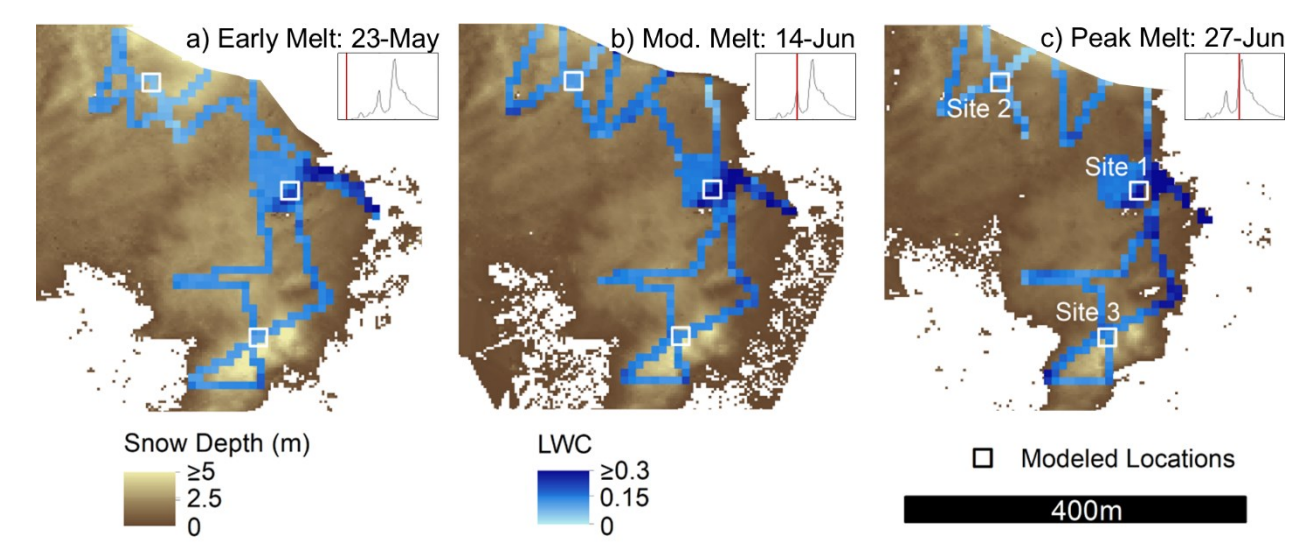


Figure 6. Observed snow depth and volumetric LWC for representative dates of a) early snowmelt prior to observable runoff, b) moderate snowmelt during the rising limb of the hydrograph, and c) peak snowmelt immediately prior to peak runoff. Insets indicated the timing of each observation relative to the observed hydrograph at the SDL stream gage. For visual purposes, LWC was resampled to a 10 m raster and LWC was only calculated along GPR transects.

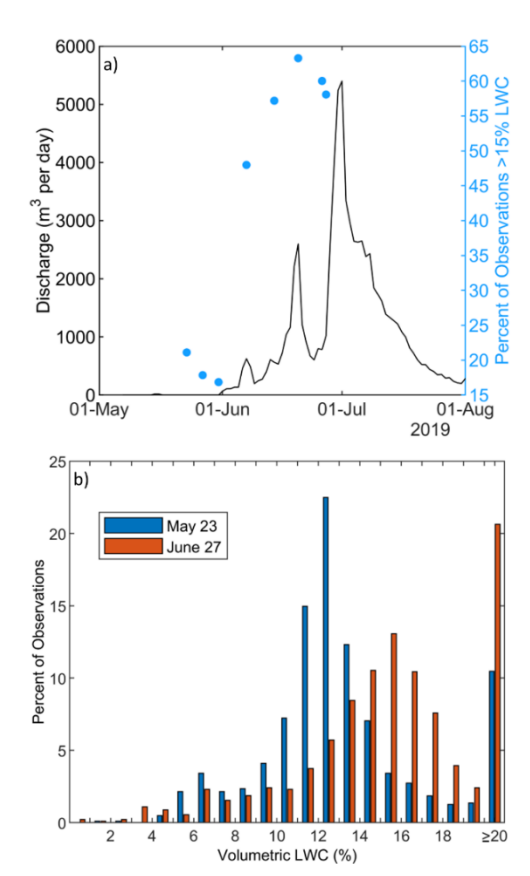


Figure 7. (a) Observed discharge at the SDL stream gauge and the percent of observed snowpack volumetric LWC that was > 15%. (b) histogram of volumetric LWC observations for May 23 and June 27.

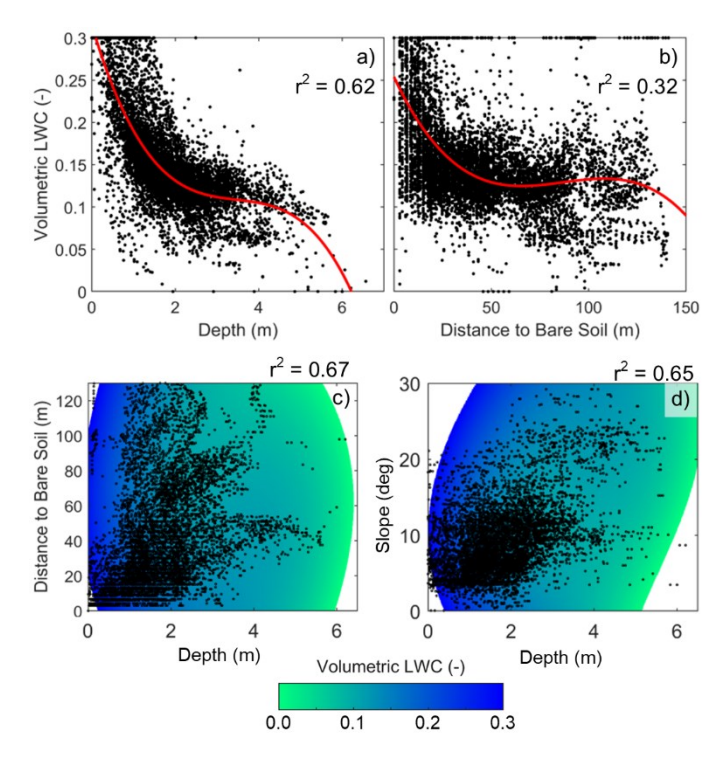


Figure 8. Third order polynomial regressions for (a) snow depth vs. θ_w , (b) distance to bare soil vs θ_w , (c) snow depth and distance to bare soil vs. θ_w , and (d) snow depth and ground surface slope vs. θ_w . The associated \mathbf{r}^2 values are given for each regression and all regressions are shown to a maximum θ_w of 0.3.



999

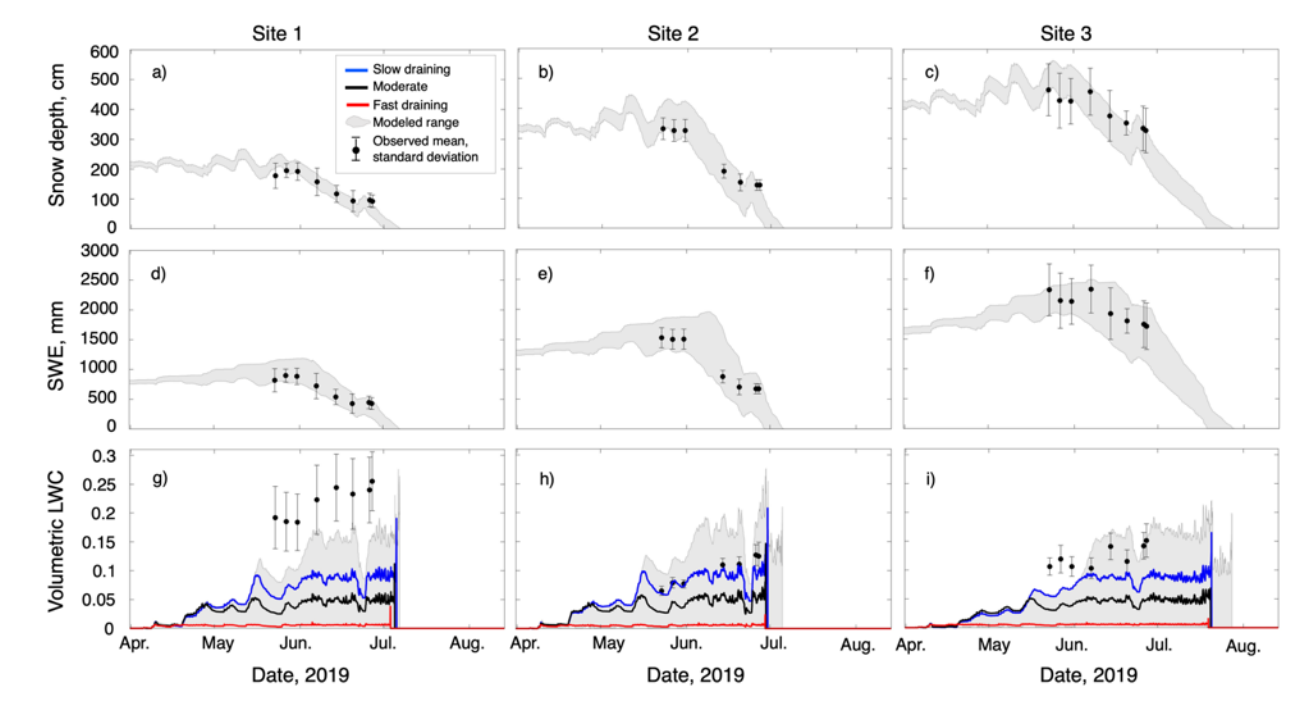


Figure 9. At each of the three study sites (panel columns), simulations and observations of snow depth (a-c), snow water equivalent (d-f), and volumetric liquid water content (g-i). Mean observations are indicated as a point with whiskers extending one standard deviation calculated based on a 20 m by 20 m box centered on the modeled locations. Simulations are shown as the range (gray shading) of 18 parameter sensitivity runs. Three example simulations (slow, moderate, and fast draining) are shown as the blue, black and red lines in the bottom panels.

1002

1003

Site 1 Site 2 Site 3 b) c) 5 layer 100 layer Mean absolute error, LWC 0.2 0.2 0.2 0.15 0.15 0.15 0.1 0.1 0.1 0.05 0.05 0 2 9 4 8 7 6 2 Simulation ID Simulation ID Simulation ID

Figure 10. Mean absolute error in SUMMA simulations of volumetric liquid water content, cm cm⁻³, at each of the three sites (panel columns). Errors (y-axis) are ranked by simulation ID (x-axis; ranking is lowest to highest, left to right) for the five-layer snow model (gray bars). The error accompanying the five-layer ranked simulation ID is also shown for the 100-layer snow model (blue bars).

a) Ponding on ice lense formed from previous drift surface

b) Saturation excess through-snow flow

c) Diversions across layer interfaces

Stream

d) Advancement of lateral wetting front faster in highly permeable snow

e) Infiltration excess from accumulation of flowpaths

Figure 11. Conceptual diagram showing the meltwater flow through-snow processes that occur including: a) ponding water on ice lenses, b) saturation excess through-snow flow, c) diversion of flowpaths along stratigraphic layers (i.e. hydraulic barriers), d) lateral advancing of a wetting front, and e) infiltration excess as a result of focused infiltration.

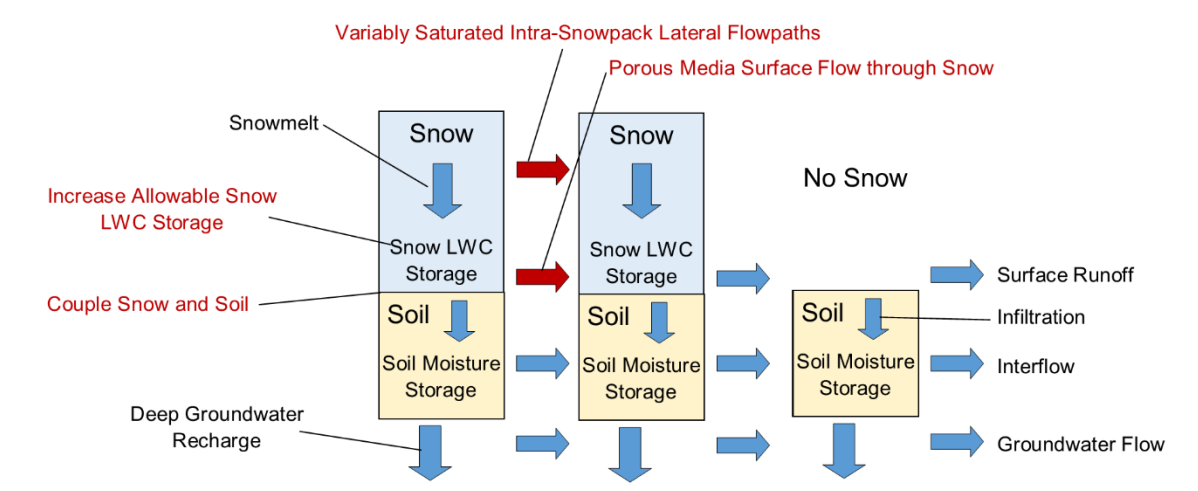


Figure 12. Visualizations of hydrologic model structure that is recommended for further investigation based on the present study that adds connectivity between the snowpack and soil. Changes to the structure from Figure 1 are indicated in red.